Science Advances
AAAS

Supplementary Materials for

Marine emissions of methanethiol increase aerosol cooling in the Southern Ocean

Charel Wohl *et al.*

Corresponding author: Rafel Simó, rsimo@icm.csic.es; Alfonso Saiz-Lopez, a.saiz@csic.es

Sci. Adv. **10**, eadq2465 (2024)
DOI: 10.1126/sciadv.adq2465

This PDF file includes:

Supplementary Materials

Supplementary Methods

Empirical model performance

Fig. S7a shows the regression of the predicted methanethiol concentrations against the observation-based training dataset, for a regime cut-off temperature of 8 °C. This illustrates that the model has been trained well on the available data. Fig. S7b indicates that the model overestimates methanethiol at low concentrations (below 0.25 nmol dm^{-3}) and generally underestimates concentrations above 3 nmol dm^{-3}, though these extremely high concentrations only occur at 2.5 % of the data points used for model development. A regression plot of the residuals against other in situ variables (Fig. S7c,d,e) does not support the inclusion of other co-sampled variables. Mean (± 95 % confidence interval) performance parameters of the model ensemble with 8 to 12 °C varying temperature cut-offs are: root mean square error (RMSE) 0.376 (0.004) nmol dm^{-3}, mean absolute error (MAE) 0.254 (0.002) nmol dm^{-3}, mean bias (meanBias) 0.030 (0.004) nmol dm^{-3}.

The model could probably be improved in terms of precision, as testified by a relative MAE of 52%. The model's relative MAE is not substantially worse than the methanethiol measurement error in the observations, estimated at 15 – 30 % across all campaigns and measurement techniques. In summary, the model seems to be highly accurate but could be improved in terms of precision, which implies that it is better suited for large-scale estimates.

Statistical validation of the empirical model

As done for determining the temperature cut-off, we employed a random subsampling method to validate the model, keeping the temperature threshold at 8 °C. The model was trained on a randomly selected subset of 80 % of the observations and used to predict the remaining, "unseen" 20 % of the dataset. This process is repeated for a total of 5,000 simulations. Model coefficients and skill metrics are shared here (Fig. S8). Scatter plots of the randomly generated coefficients and the predicted vs observation-based training dataset indicate a negative correlation. This is because of the effect of noise on regression statistics. In the high MeSH:DMS regime, specific validation runs result in low R^2 values. This may indicate a limited number of outliers in this category. It is worth noting that this scenario only applies to a small number of data points and does not seem to substantially impact the overall model validity. The histograms illustrating the 5,000 randomly generated skill metrics are notably centred around the metrics obtained in the ensemble runs with varying temperature cut-offs. Therefore, these metrics can reliably be employed to gauge model performance.

MeSH and DMS flux calculations

We used the climatological maps of MeSH seawater concentrations to calculate the sea-to-air flux of MeSH. We use the solubility for methanethiol recommended by Burkholder et al. (*54*):

$$H^{cc}(T) = e^{-12.42+\frac{3420}{t+273.15}} \times \frac{1}{0.04087} \qquad \text{Eqn. 1}$$

where $H^{CC}(T)$ is the dimensionless water over air solubility of methanethiol as a function of ambient seawater temperature (T) in °C. The factor of $\frac{1}{0.04087}$ is used here to convert the units from $\frac{M}{atm}$ to the dimensionless water over air form of the solubility. The waterside Schmidt number of DMS was calculated as per Johnson (*60*). We assume the Schmidt number of methanethiol (Sc_{MeSH}) has the same temperature dependence as DMS and scale them at 25 °C (listed in ref. (*61*)):

$$Sc_{MeSH}(T) = 2815.7 - 204.01T + 9.09T^2 - 0.27T^3 + 0.004T^4 \qquad \text{Eqn. 2}$$

The waterside transfer velocity of DMS and methanethiol (k_w) was calculated as a linear function of friction velocity (*62*). At wind speeds lower than 2 m s^{-1}, k_w was set to 1.1 cm h^{-1}. Friction velocity was calculated according to Johnson (*60*). Airside transfer velocities are calculated using the parametrisation by Yang et al. (*63*). For each compound "i", the total ocean-to-atmosphere transfer velocity was calculated as the reciprocal sum of water ($k_{w,i}$) and air ($k_{a,i}$) transfer velocities (Eqn. 3):

$$k_i = \left[\frac{1}{k_{w,i}} + \frac{H}{k_{a,i}}\right]^{-1} \qquad \text{Eqn. 3}$$

Finally, gas fluxes were calculated using k_i, seawater gas concentrations ($C_{w,i}$) and fractional sea ice cover ($f_{ice} as 0 - 1$):

$$\begin{aligned} F_i &= k_i \times (C_{w,i} - H_i \times C_{a,i}) \times (1 - f_{ice}); \qquad & f_{ice} \leq 0.85 \\ F_i &= 0 & f_{ice} \gg 0.85 \end{aligned} \qquad \text{Eqn. 4}$$

Airside DMS concentration is considered to be zero for consistency with previous climatologies. Air-side methanethiol can be considered to be zero in the flux calculation on this global scale because methanethiol is likely consistently highly supersaturated in the surface ocean as suggested by measurements (*23*, *26*) (i), and methanethiol has a very short lifetime in the atmosphere (ii). Given (i) and (ii) it is unlikely that atmospheric transport from anthropogenic sources (*64*) substantially impacts the calculated flux. The sea-to-air flux was scaled linearly to the open water fraction up to 85 % ice. Above this threshold, we assumed no air-sea exchange was occurring.

Global fluxes were calculated at 1°x1° monthly resolution using gridded MeSH and DMS sea-surface concentrations. Wind speeds were taken from MERRA_v2 hourly 10-m wind speed, which was used to calculate a monthly climatology for the 1998-2022 period. Observational climatologies of sea ice cover and SST were obtained from the Hadley Centre HadISST gridded database (*65*) over the 1998-2022 period. Based on the land mask of the Community Earth System Model (CESM) used in this work, coastal pixels composed of a mixture of continent and ocean were treated as terrestrial, thus assuming no air-sea exchange.

Global monthly 1°x1° fields of sea-surface DMS concentration were obtained from the most updated climatology (*14*) and used to calculate global DMS emissions. These fields were also used in combination with the observational SST climatology and the General Bathymetric Chart of the Oceans to produce MeSH concentration fields, according to the threshold-based regression model. Rather than using a single set of model coefficients to estimate global monthly MeSH fields, we produced a 100-member ensemble to better account for uncertainty in the MeSH statistical model. To this end, we randomly drew 20 sets of the model coefficients fitted at different cut-off temperatures between 8 and

12°C (5 cut-offs x 20 coefficient sets = 100 coefficient sets). Finally, the ensemble mean was used to calculate global MeSH emissions. We also computed the ensemble median, standard deviation and relevant quartiles to quantify uncertainty in climatological MeSH fields and to enable sensitivity analyses with the CAM-Chem model. As expected, MeSH fields show larger spread in grid cells whose SST is in the 8–12°C range, reflecting uncertainty in their assignment to the high or low MeSH:DMS regime depending on the temperature cut-off used.

It should be noted that our approach is not designed to quantify the uncertainty in global emissions, but to robustly quantify the effect of adding MeSH emission to a DMS-only baseline. The global DMS emission estimated here (23.5 TgS y^{-1}) is within ± 20% of the most recent estimates obtained with various approaches (*14*, *66*, *67*), and incorporates an updated gas exchange parametrisation with linear wind-speed dependence. Previous studies had reported wider uncertainty ranges for global DMS emission (*68*, *69*), but the extreme values (9 to 34 TgS y^{-1}) resulted from the use of "legacy" gas exchange parametrisations that nowadays are regarded as outdated and/or inappropriate for DMS (*62*, *70*). These "legacy" parametrisations keep being used to enable comparison with older studies (*67*, *69*). While uncertainties in global MeSH and DMS emissions certainly need further assessment, here we provide our best central estimates for their global emissions and ensuing atmospheric effects.

Radiative effect

The radiative effect (RE) induced by the MeSH emission was computed (*33*, *71*) as the change in the net radiative balance induced by the sulfate aerosol direct effect between 'MeSH' and 'noMeSH' simulations, which include and omit MeSH emission respectively. The net radiative balance (RB) is obtained as the difference between the top-of-model net solar flux (FSNT) and net longwave flux (FLNT) for all-sky conditions as follows:

$$RB = FSNT - FLNT \qquad \text{Eqn. 5}$$

The MeSH-induced SO_4^{2-} direct RE was then calculated as follows:

$$\Re_{SO4} = RB_{SO4}^{MeSH} - RB_{SO4}^{noMeSH} \qquad \text{Eqn. 6}$$

The component of the radiative balance attributed to the direct effect of sulfate aerosol (RB_{SO4}) was calculated using model diagnostics based on a single-addition and single-subtraction analysis (*72*). This approach allows constraining the individual radiative contribution of sulfate aerosol from the total radiative budget using the Rapid Radiative Transfer Model for Global circulation models (RRTMG) radiative scheme in CESM (*73*). These diagnoses provide the contribution of individual radiatively active species by adding or removing them from the full set of climate forcing agents. This way, following the single-addition approach, we computed the direct radiative contribution of sulfate aerosol by subtracting the FSNT and FLNT variables from the RRTMG diagnosis that neglects the contribution from all climate forcing agents (dNoForz) from the diagnosis that considers sulfate aerosol as the only radiatively active component (dSO4) (Eqn. 6). Additionally, the FSNT and FLNT variables of the diagnosis omitting sulfate aerosol from the full set of forcers (dNoSO4) were subtracted from the diagnosis considering all radiative forcing (dAllForz), following the single-subtraction approach (Eqn. 6):

$$\Re^{sa}_{SO4} = RB_{dSO4} - RB_{dNoForz} \quad \text{Eqn. 7}$$

$$\Re^{ss}_{SO4} = RB_{dAllForz} - RB_{dNoSO4} \quad \text{Eqn. 8}$$

Combining Eqns. 7 and 8 with Eqn. 6, we obtained the respective single-addition and single-subtraction approaches of the MeSH-induced SO_4^{2-} direct RE:

$$\Re^{sa}_{SO4} = (RB_{dSO4} - RB_{dNoForz})^{MeSH} - (RB_{dSO4} - RB_{dNoForz})^{noMeSH} \quad \text{Eqn. 9}$$

$$\Re^{ss}_{SO4} = (RB_{dAllForz} - RB_{dNoSO4})^{MesH} - (RB_{dAllForz} - RB_{dNoSO4})^{noMesH} \quad \text{Eqn. 10}$$

Following Lacis *et al.* (*72*), a normalized RE_{SO4} was then calculated from the values obtained with the single-addition and single-subtraction approaches, respectively using the recommended 0.428 and 0.572 weighting factors.

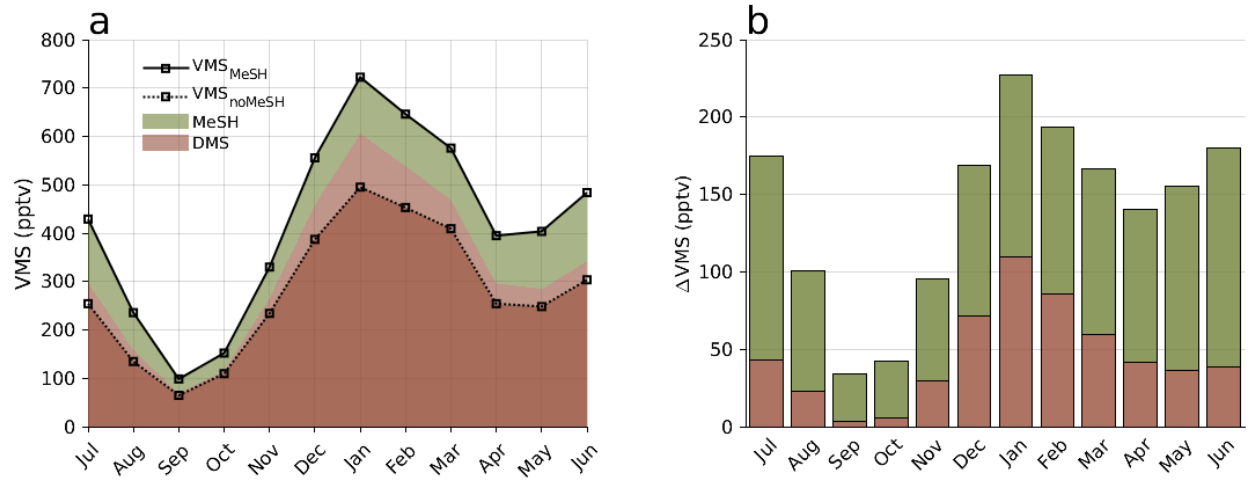

Fig. S1. Annual cycle of the increase in tropospheric VMS concentrations accounted for by MeSH emission in the Southern Ocean. a. Monthly VMS concentrations averaged below 850 hPa generated by the 'MeSH' (solid line) and 'noMeSH' (dashed line) simulations. **b**. Their increment, decomposed into the MeSH (green shade) and DMS (brown shade) contributions.

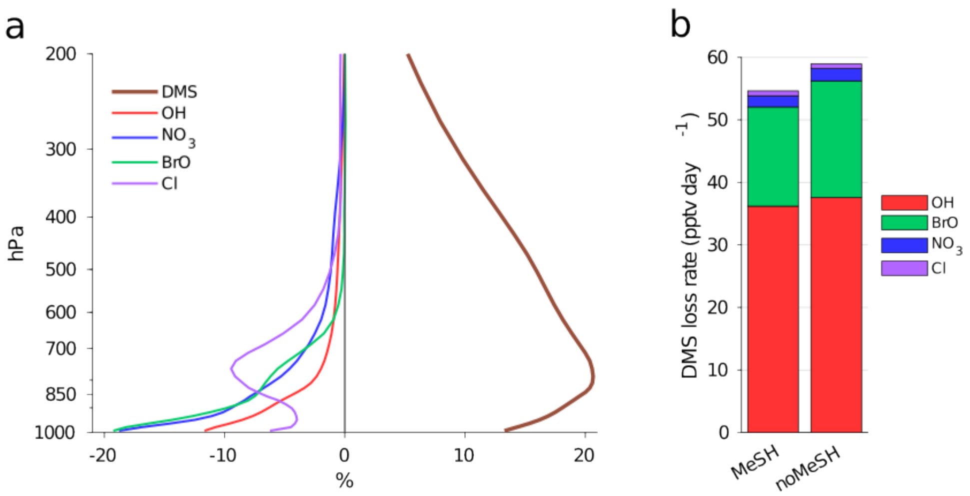

Fig. S2. Impact of adding MeSH on the oxidation and vertical distribution of DMS. **a.** Vertical profiles of the relative changes in the burdens of DMS and its oxidants (OH, NO_3, BrO and Cl) over the Southern Ocean represented by the 'MeSH' simulation. **b.** Contribution of individual oxidants to the total DMS loss rate averaged in the Southern Ocean lower troposphere (below 850 hPa) in the 'MeSH' and 'noMeSH' simulations.

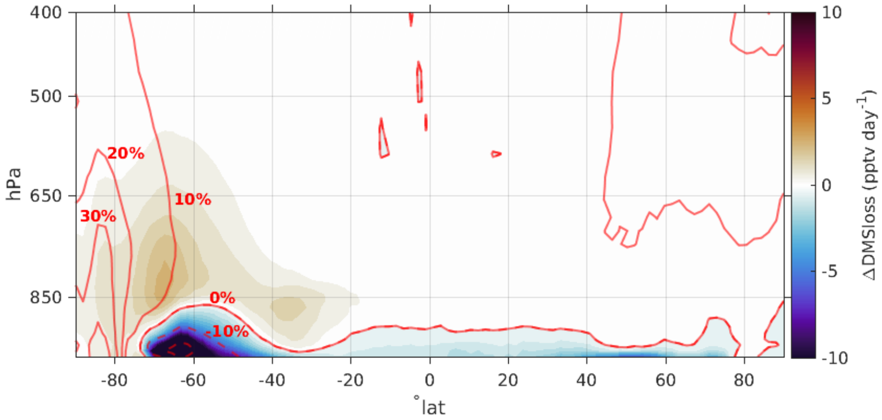

Fig. S3. Change of the annual-mean DMS loss rate accounted for by MeSH emission. Absolute (pptv day^{-1}; shade) and relative (%; red contours) shift of the zonal-mean chemical loss rate of DMS attributed to MeSH emission.

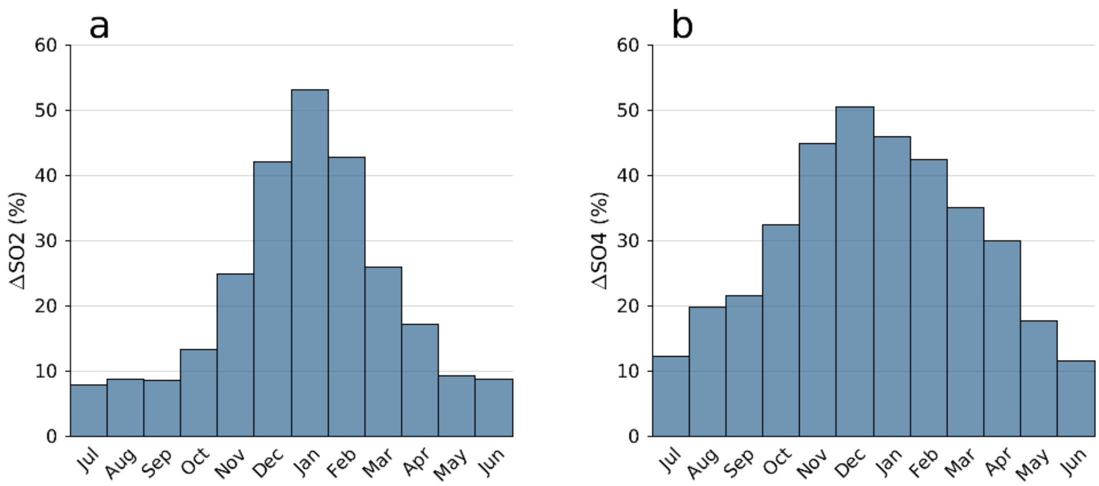

Fig. S4. Annual variation of additional SO_2 and SO_4^{2-} over the Southern Ocean accounted for by MeSH emission. Monthly relative increments of the (**a**) SO_2 and (**b**) SO_4^{2-} burdens averaged in the Southern Ocean lower troposphere (below 850 hPa).

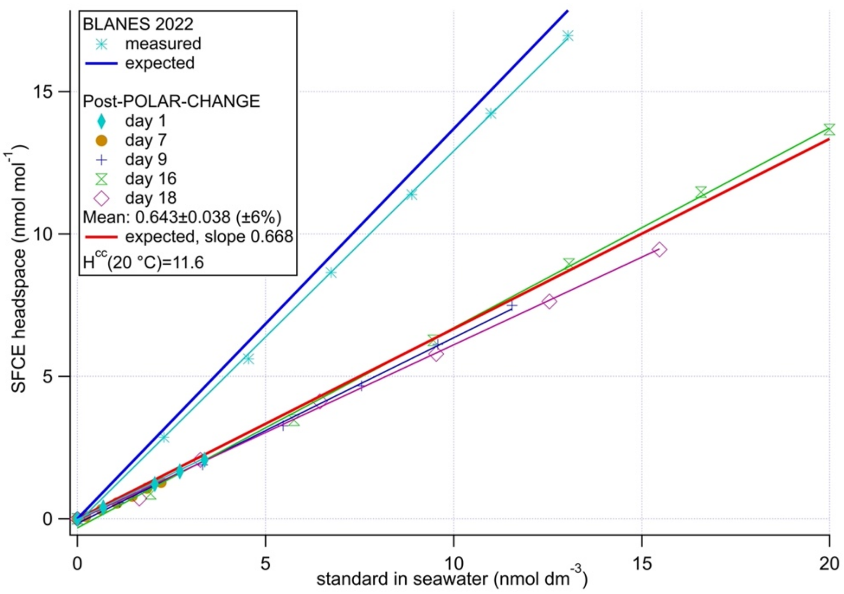

Fig. S5. Comparison of expected and measured methanethiol equilibrator headspace mixing ratios. Two sets of calibrations in seawater are presented: BLANES2022 and post-POLAR-CHANGE. The figure illustrates that slightly different factors were applied in both datasets to convert from equilibrator headspace mixing ratios (nmol mol^{-1}) to seawater concentrations (nmol dm^{-3}). This is due to different air and water flows into the equilibrator during both deployments.

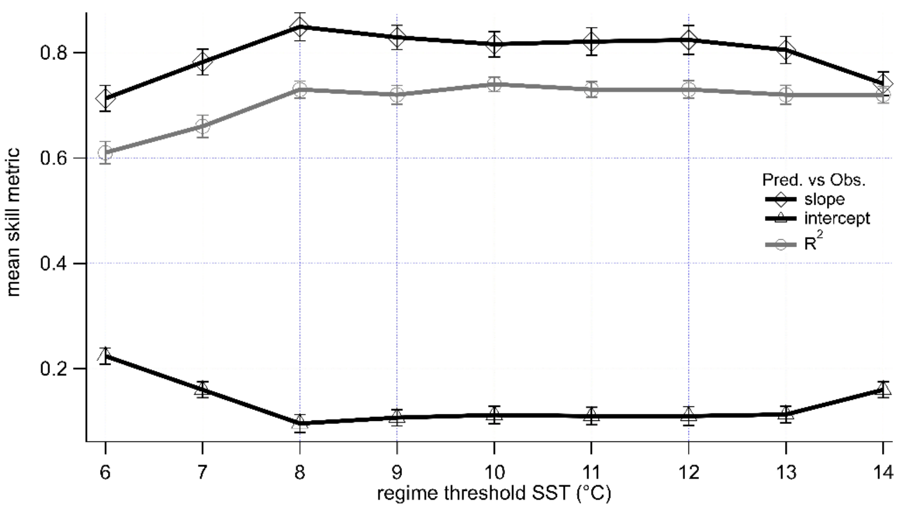

Fig. S6. Empirical model performance as a function of using different temperature cut-offs. Mean slope, intercept (type 2 fit) and R^2 value of the predicted vs observed values using different temperature cut-offs. Error bars represent the 95 % confidence interval.

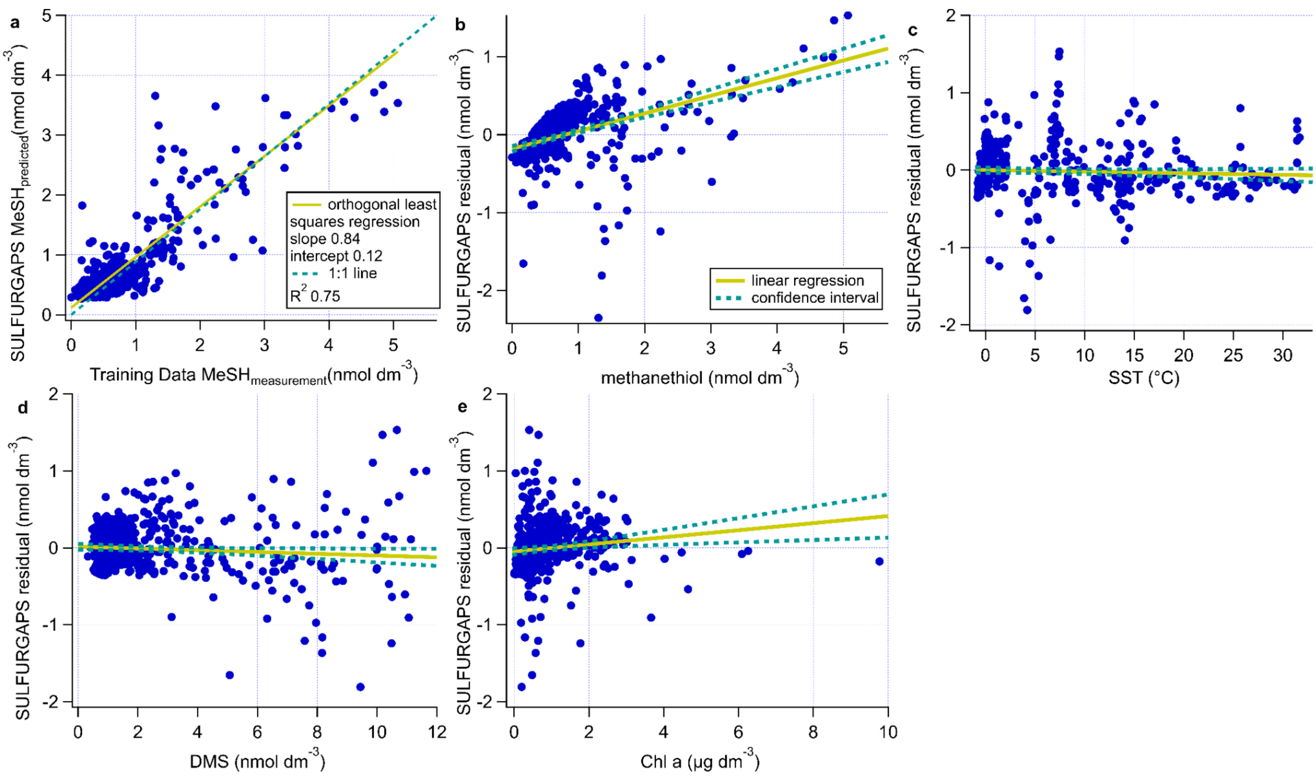

Fig. S7. Empirical model performance for regime temperature cut-off at 8 °C. **a.** Orthogonal least squares regression analysis (type 2 regression) of the predictions against the observations of methanethiol used to train the empirical model. To account for error in the x- (analytical measurement error) and y-axis (model error), we adopt a type 2 regression for the slope and intercept shown. The R^2 value was calculated using a standard linear regression (type 1 regression). **b-e**. Linear regression and confidence intervals of the model residual against other variables, namely MeSH, SST, DMS and Chl *a*.

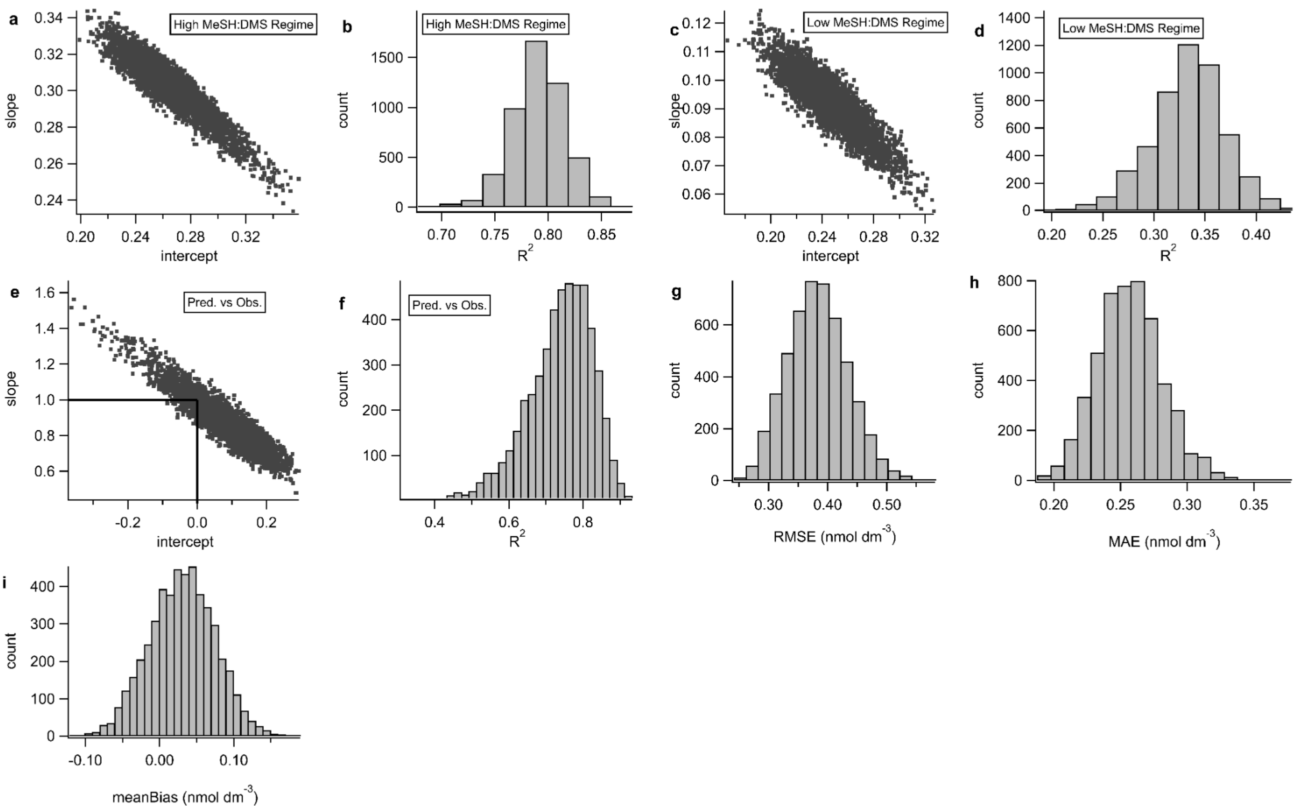

Fig. S8. Validation of the empirical model based on a cut-off SST of 8 °C. a-d, Scatter plots of the intercept vs slope of the high and low MeSH:DMS regimes plus histograms of the R^2. **e-f,** Scatter plot of the slope vs intercept of the predicted vs observation-based training dataset (type 2 fit) plus a histogram of the R^2. Target values for slope (=1) and intercept (=0) shown as lines in **e**. **g-i,** Histograms of the performance statistics (RMSE, MAE, meanBias).

Table S1: Chemical scheme of MeSH-related reactions included in the CAM-Chem simulations.

Reaction	Rate
MeSH + OH → CH_3S + H_2O	$9.9 \times 10^{-12} \times \exp(360/T)$
MeSH + BrO → CH_3S + HOBr	$2.2 \times 10^{-15} \times \exp(830/T)$
MeSH + NO_3 → CH_3S + HNO_3	9.2×10^{-13}
MeSH + Cl → CH_3S + HCl	$1.2 \times 10^{-10} \times \exp(150/T)$
CH_3S + NO_2 → CH_3SO + NO	$6.0 \times 10^{-11} \times \exp(240/T)$
CH_3S + O_3 → CH_3SO + O_2	$1.15 \times 10^{-12} \times \exp(430/T)$
CH_3S + O_2 → CH_3SOO	$1.2 \times 10^{-16} \times \exp(1580/T)$
CH_3SO + O_2 → $CH_3S(O)OO$	$3.12 \times 10^{-16} \times \exp(1580/T)$
CH_3SO + O_3 → CH_3O_2 + SO_2	4.0×10^{-11}
CH_3SO + NO_2 → 0.75×$CH_3S(O)O$ + 0.25×CH_3O_2 + 0.25×SO_2 + NO	1.2×10^{-11}
CH_3SOO + NO → NO_2 + CH_3SO	1.1×10^{-11}
CH_3SOO + NO_2 → NO_3 + CH_3SO	2.2×10^{-11}
CH_3SOO → CH_3O_2 + SO_2	$5.6 \times 10^{16} \times \exp(-10870/T)$
CH_3SOO → CH_3S	$3.5 \times 10^{10} \times \exp(-3560/T)$
$CH_3S(O)O$ + O_3 → CH_3SO_3	3.0×10^{-13}
CH_3SO_3 + HO_2 → CH_3SO_3H + O_3	5.0×10^{-11}
CH_3SO_3 → CH_3O_2 + SO_3	$5.0 \times 10^{13} \times \exp(-9946/T)$
$CH_3S(O)O$ + O_3 → CH_3O_2 + SO_2	$5.0 \times 10^{13} \times \exp(-9673/T)$

REFERENCES AND NOTES

1. M. A. Moran, B. P. Durham, Sulfur metabolites in the pelagic ocean. *Nat. Rev. Microbiol.* **17**, 665–678 (2019).

2. F. E. Hopkins, S. D. Archer, T. G. Bell, P. Suntharalingam, J. D. Todd, The biogeochemistry of marine dimethylsulfide. *Nat. Rev. Earth Environ.* **4**, 361–376 (2023).

3. P. A. Matrai, M. D. Keller, Total organic sulfur and dimethylsulfoniopropionate in marine phytoplankton: Intracellular variations. *Mar. Biol.* **119**, 61–68 (1994).

4. M. Galí, E. Devred, M. Levasseur, S.-J. Royer, M. Babin, A remote sensing algorithm for planktonic dimethylsulfoniopropionate (DMSP) and an analysis of global patterns. *Remote Sens. Environ.* **171**, 171–184 (2015).

5. R. Simó, Production of atmospheric sulfur by oceanic plankton: Biogeochemical, ecological and evolutionary links. *Trends Ecol. Evol.* **6**, 287–294 (2001).

6. R. P. Kiene, Production of methanethiol from dimethylsulfoniopropionate in marine surface waters. *Mar. Chem.* **54**, 69–83 (1996).

7. R. J. Charlson, J. E. Lovelock, M. O. Andreae, S. G. Warren, Oceanic phytoplankton, atmospheric sulphur, cloud albedo and climate. *Nature* **326**, 655–661 (1987).

8. A. L. Hodshire, P. Campuzano-Jost, J. K. Kodros, B. Croft, B. A. Nault, J. C. Schroder, J. L. Jimenez, J. R. Pierce, The potential role of methanesulfonic acid (MSA) in aerosol formation and growth and the associated radiative forcings. *Atmos. Chem. Phys.* **19**, 3137–3160 (2019).

9. M. O. Andreae, P. J. Crutzen, Atmospheric aerosols: Biogeochemical sources and role in atmospheric chemistry. *Science* **276**, 1052–1058 (1997).

10. M. D. Mallet, R. S. Humphries, S. L. Fiddes, S. P. Alexander, K. Altieri, H. Angot, N. Anilkumar, T. Bartels-Rausch, J. Creamean, M. Dall'Osto, A. Dommergue, M. Frey, S. Henning, D. Lannuzel, R. Lapere, G. G. Mace, A. S. Mahajan, G. M. McFarquhar, K. M. Meiners, B. Miljevic, I. Peeken, A. Protat, J. Schmale, N. Steiner, K. Sellegri, R. Simó, J. L.

Thomas, M. D. Willis, V. H. L. Winton, M. T. Woodhouse, Untangling the influence of Antarctic and Southern Ocean life on clouds. *Elem. Sci. Anth.* **11**, 00130 (2023).

11. D. T. McCoy, S. M. Burrows, R. Wood, D. P. Grosvenor, S. M. Elliott, P.-L. Ma, P. J. Rasch, D. L. Hartmann, Natural aerosols explain seasonal and spatial patterns of Southern Ocean cloud albedo. *Sci. Adv.* **1**, e1500157 (2015).

12. K. M. Fung, C. L. Heald, J. H. Kroll, S. Wang, D. S. Jo, A. Gettelman, Z. Lu, X. Liu, R. A. Zaveri, E. C. Apel, D. R. Blake, J.-L. Jimenez, P. Campuzano-Jost, P. R. Veres, T. S. Bates, J. E. Shilling, M. Zawadowicz, Exploring dimethyl sulfide (DMS) oxidation and implications for global aerosol radiative forcing. *Atmos. Chem. Phys.* **22**, 1549–1573 (2022).

13. W. Aas, A. Mortier, V. Bowersox, R. Cherian, G. Faluvegi, H. Fagerli, J. Hand, Z. Klimont, C. Galy-Lacaux, C. M. B. Lehmann, C. L. Myhre, G. Myhre, D. Olivié, K. Sato, J. Quaas, P. S. P. Rao, M. Schulz, D. Shindell, R. B. Skeie, A. Stein, T. Takemura, S. Tsyro, R. Vet, X. Xu, Global and regional trends of atmospheric sulfur. *Sci. Rep.* **9**, 953 (2019).

14. S. Hulswar, R. Simó, M. Galí, T. G. Bell, A. Lana, S. Inamdar, P. R. Halloran, G. Manville, A. S. Mahajan, Third revision of the global surface seawater dimethyl sulfide climatology (DMS-Rev3). *Earth Syst. Sci. Data* **14**, 2963–2987 (2022).

15. R. P. Kiene, L. J. Linn, The fate of dissolved dimethylsulfoniopropionate (DMSP) in seawater: Tracer studies using ^{35}S-DMSP. *Geochim. Cosmochim. Acta* **64**, 2797–2810 (2000).

16. M. Galí, R. Simó, A meta-analysis of oceanic DMS and DMSP cycling processes: Disentangling the summer paradox. *Global Biogeochem. Cycles* **29**, 496–515 (2015).

17. C. R. Reisch, M. J. Stoudemayer, V. A. Varaljay, I. J. Amster, M. A. Moran, W. B. Whitman, Novel pathway for assimilation of dimethylsulphoniopropionate widespread in marine bacteria. *Nature* **473**, 208–211 (2011).

18. M. Landa, A. S. Burns, B. P. Durham, K. Esson, B. Nowinski, S. Sharma, A. Vorobev, T. Nielsen, R. P. Kiene, M. A. Moran, Sulfur metabolites that facilitate oceanic phytoplankton–bacteria carbon flux. *ISME J.* **13**, 2536–2550 (2019).

19. J. Sun, J. D. Todd, J. C. Thrash, Y. Qian, M. C. Qian, B. Temperton, J. Guo, E. K. Fowler, J. T. Aldrich, C. D. Nicora, M. S. Lipton, R. D. Smith, P. De Leenheer, S. H. Payne, A. W. B. Johnston, C. L. Davie-Martin, K. H. Halsey, S. J. Giovannoni, The abundant marine bacterium Pelagibacter simultaneously catabolizes dimethylsulfoniopropionate to the gases dimethyl sulfide and methanethiol. *Nat. Microbiol.* **1**, 16065 (2016).

20. H. Schäfer, Ö. Eyice, Microbial cycling of methanethiol. *Curr. Issues Mol. Biol.* **33**, 173–182 (2019).

21. H. Bürgmann, E. C. Howard, W. Ye, F. Sun, S. Sun, S. Napierala, M. A. Moran, Transcriptional response of Silicibacter pomeroyi DSS-3 to dimethylsulfoniopropionate (DMSP). *Environ. Microbiol.* **9**, 2742–2755 (2007).

22. X.-Y. He, N.-H. Liu, J.-Q. Liu, M. Peng, Z.-J. Teng, T.-J. Gu, X.-L. Chen, Y. Chen, P. Wang, C.-Y. Li, J. D. Todd, Y.-Z. Zhang, X.-Y. Zhang, SAR92 clade bacteria are potentially important DMSP degraders and sources of climate-active gases in marine environments. *mBio* **14**, e01467-23 (2023).

23. A. J. Kettle, T. S. Rhee, M. von Hobe, A. Poulton, J. Aiken, M. O. Andreae, Assessing the flux of different volatile sulfur gases from the ocean to the atmosphere. *J. Geophys. Res. Atmos.* **106**, 12193–12209 (2001).

24. V. Gros, B. Bonsang, R. Sarda-Estève, A. Nikolopoulos, K. Metfies, M. Wietz, I. Peeken, Concentrations of dissolved dimethyl sulfide (DMS), methanethiol and other trace gases in context of microbial communities from the temperate Atlantic to the Arctic Ocean. *Biogeosciences* **20**, 851–867 (2023).

25. S. J. Lawson, C. S. Law, M. J. Harvey, T. G. Bell, C. F. Walker, W. J. de Bruyn, E. S. Saltzman, Methanethiol, dimethyl sulfide and acetone over biologically productive waters in the southwest Pacific Ocean. *Atmos. Chem. Phys.* **20**, 3061–3078 (2020).

26. G. A. Novak, D. B. Kilgour, C. M. Jernigan, M. P. Vermeuel, T. H. Bertram, Oceanic emissions of dimethyl sulfide and methanethiol and their contribution to sulfur dioxide production in the marine atmosphere. *Atmos. Chem. Phys.* **22**, 6309–6325 (2022).

27. D. B. Kilgour, C. M. Jernigan, S. Zhou, E. Brito de Azevedo, J. Wang, M. A. Zawadowicz, T. H. Bertram, Contribution of speciated monoterpenes to secondary aerosol in the Eastern North Atlantic. *ACS EST Air* **1**, 789–800 (2024).

28. D. B. Kilgour, G. A. Novak, J. S. Sauer, A. N. Moore, J. Dinasquet, S. Amiri, E. B. Franklin, K. Mayer, M. Winter, C. K. Morris, T. Price, F. Malfatti, D. R. Crocker, C. Lee, C. D. Cappa, A. H. Goldstein, K. A. Prather, T. H. Bertram, Marine gas-phase sulfur emissions during an induced phytoplankton bloom. *Atmos. Chem. Phys.* **22**, 1601–1613 (2022).

29. Intergovernmental Panel On Climate Change, *Climate Change 2021–The Physical Science Basis: Working Group I Contribution to the Sixth Assessment Report of the Intergovernmental Panel on Climate Change* (Cambridge Univ. Press, ed. 1, 2023).

30. C. Wohl, Q. Güell-Bujons, Y. M. Castillo, A. Calbet, R. Simó, Volatile organic compounds released by *Oxyrrhis marina* grazing on *Isochrysis galbana*. *Oceans* **4**, 151–169 (2023).

31. O. R. Flöck, M. O. Andreae, Photochemical and non-photochemical formation and destruction of carbonyl sulfide and methyl mercaptan in ocean waters. *Mar. Chem.* **54**, 11–26 (1996).

32. V. S. Ulshöfer, O. R. Flock, G. Uher, M. O. Andreae, Photochemical production and air-sea exchange of carbonyl sulfide in the eastern Mediterranean Sea. *Mar. Chem.* **53**, 25–39 (1996).

33. A. Saiz-Lopez, R. P. Fernandez, Q. Li, C. A. Cuevas, X. Fu, D. E. Kinnison, S. Tilmes, A. S. Mahajan, J. C. Gómez Martín, F. Iglesias-Suarez, R. Hossaini, J. M. C. Plane, G. Myhre, J.-F. Lamarque, Natural short-lived halogens exert an indirect cooling effect on climate. *Nature* **618**, 967–973 (2023).

34. J.-F. Lamarque, L. K. Emmons, P. G. Hess, D. E. Kinnison, S. Tilmes, F. Vitt, C. L. Heald, E. A. Holland, P. H. Lauritzen, J. Neu, J. J. Orlando, P. J. Rasch, G. K. Tyndall, CAM-chem: Description and evaluation of interactive atmospheric chemistry in the Community Earth System Model. *Geosci. Model Dev.* **5**, 369–411 (2012).

35. G. Myhre, W. Aas, R. Cherian, W. Collins, G. Faluvegi, M. Flanner, P. Forster, Ø. Hodnebrog, Z. Klimont, M. T. Lund, J. Mülmenstädt, C. L. Myhre, D. Olivié, M. Prather, J. Quaas, B. H. Samset, J. L. Schnell, M. Schulz, D. Shindell, R. B. Skeie, T. Takemura, S. Tsyro, Multi-model simulations of aerosol and ozone radiative forcing due to anthropogenic emission changes during the period 1990–2015. *Atmos. Chem. Phys.* **17**, 2709–2720 (2017).

36. Y. Yang, H. Wang, S. J. Smith, R. Easter, P.-L. Ma, Y. Qian, H. Yu, C. Li, P. J. Rasch, Global source attribution of sulfate concentration and direct and indirect radiative forcing. *Atmos. Chem. Phys.* **17**, 8903–8922 (2017).

37. A. Rap, C. E. Scott, D. V. Spracklen, N. Bellouin, P. M. Forster, K. S. Carslaw, A. Schmidt, G. Mann, Natural aerosol direct and indirect radiative effects. *Geophys. Res. Lett.* **40**, 3297–3301 (2013).

38. A. Bodas-Salcedo, K. D. Williams, M. A. Ringer, I. Beau, J. N. S. Cole, J.-L. Dufresne, T. Koshiro, B. Stevens, Z. Wang, T. Yokohata, Origins of the solar radiation biases over the Southern Ocean in CFMIP2 models. *J. Clim.* **27**, 41–56 (2014).

39. S. L. Fiddes, A. Protat, M. D. Mallet, S. P. Alexander, M. T. Woodhouse, Southern Ocean cloud and shortwave radiation biases in a nudged climate model simulation: Does the model ever get it right? *Atmos. Chem. Phys.* **22**, 14603–14630 (2022).

40. A. J. Schuddeboom, A. J. McDonald, The Southern Ocean radiative bias, cloud compensating errors, and equilibrium climate sensitivity in CMIP6 models. *J. Geophys. Res. Atmos.* **126**, e2021JD035310 (2021).

41. Q. Li, R. P. Fernandez, R. Hossaini, F. Iglesias-Suarez, C. A. Cuevas, E. C. Apel, D. E. Kinnison, J.-F. Lamarque, A. Saiz-Lopez, Reactive halogens increase the global methane lifetime and radiative forcing in the 21st century. *Nat. Commun.* **13**, 2768 (2022).

42. C. Wohl, Q. Li, C. A. Cuevas, R. P. Fernandez, M. Yang, A. Saiz-Lopez, R. Simó, Marine biogenic emissions of benzene and toluene and their contribution to secondary organic aerosols over the polar oceans. *Sci. Adv.* **9**, eadd9031 (2023).

43. V. Ferracci, J. Weber, C. G. Bolas, A. D. Robinson, F. Tummon, P. Rodríguez-Ros, P. Cortés-Greus, A. Baccarini, R. L. Jones, M. Galí, R. Simó, J. Schmale, N. R. P. Harris, Atmospheric isoprene measurements reveal larger-than-expected Southern Ocean emissions. *Nat. Commun.* **15**, 2571 (2024).

44. L. Bopp, O. Boucher, O. Aumont, S. Belviso, J.-L. Dufresne, M. Pham, P. Monfray, Will marine dimethylsulfide emissions amplify or alleviate global warming? A model study. *Can. J. Fish. Aquat. Sci.* **61**, 826–835 (2004).

45. A. Gabric, B. Qu, L. Rotstayn, J. Shephard, Global simulations of the impact on contemporary climate of a perturbation to the sea-to-air flux of dimethylsulfide. *Aust. Meteorol. Oceanogr. J.* **63**, 365–376 (2013).

46. S. Wang, M. E. Maltrud, S. M. Burrows, S. M. Elliott, P. Cameron-Smith, Impacts of shifts in phytoplankton community on clouds and climate via the sulfur cycle. *Global Biogeochem. Cycles* **32**, 1005–1026 (2018).

47. S. M. Vallina, R. Simó, Strong relationship between DMS and the solar radiation dose over the global surface ocean. *Science* **315**, 506–508 (2007).

48. A. Lana, R. Simó, S. M. Vallina, J. Dachs, Potential for a biogenic influence on cloud microphysics over the ocean: A correlation study with satellite-derived data. *Atmos. Chem. Phys.* **12**, 7977–7993 (2012).

49. P. K. Quinn, T. S. Bates, The case against climate regulation via oceanic phytoplankton sulphur emissions. *Nature* **480**, 51–56 (2011).

50. P. K. Quinn, D. J. Coffman, J. E. Johnson, L. M. Upchurch, T. S. Bates, Small fraction of marine cloud condensation nuclei made up of sea spray aerosol. *Nat. Geosci.* **10**, 674–679 (2017).

51. P. R. Veres, J. A. Neuman, T. H. Bertram, E. Assaf, G. M. Wolfe, C. J. Williamson, B. Weinzierl, S. Tilmes, C. R. Thompson, A. B. Thames, J. C. Schroder, A. Saiz-Lopez, A. W. Rollins, J. M. Roberts, D. Price, J. Peischl, B. A. Nault, K. H. Møller, D. O. Miller, S.

Meinardi, Q. Li, J.-F. Lamarque, A. Kupc, H. G. Kjaergaard, D. Kinnison, J. L. Jimenez, C. M. Jernigan, R. S. Hornbrook, A. Hills, M. Dollner, D. A. Day, C. A. Cuevas, P. Campuzano-Jost, J. Burkholder, T. P. Bui, W. H. Brune, S. S. Brown, C. A. Brock, I. Bourgeois, D. R. Blake, E. C. Apel, T. B. Ryerson, Global airborne sampling reveals a previously unobserved dimethyl sulfide oxidation mechanism in the marine atmosphere. *Proc. Natl. Acad. Sci. U.S.A.* **117**, 4505–4510 (2020).

52. K. Goto-Azuma, M. Hirabayashi, H. Motoyama, T. Miyake, T. Kuramoto, R. Uemura, M. Igarashi, Y. Iizuka, T. Sakurai, S. Horikawa, K. Suzuki, T. Suzuki, K. Fujita, Y. Kondo, S. Hattori, Y. Fujii, Reduced marine phytoplankton sulphur emissions in the Southern Ocean during the past seven glacials. *Nat. Commun.* **10**, 3247 (2019).

53. C. Wohl, D. Capelle, A. Jones, W. T. Sturges, P. D. Nightingale, B. G. T. Else, M. Yang, Segmented flow coil equilibrator coupled to a proton-transfer-reaction mass spectrometer for measurements of a broad range of volatile organic compounds in seawater. *Ocean Sci.* **15**, 925–940 (2019).

54. J. B. Burkholder, S. P. Sander, J. P. D. Abbatt, J. R. Barker, C. D. Cappa, J. D. Crounse, T. S. Dibble, R. E. Huie, C. E. Kolb, M. J. Kurylo, V. L. Orkin, C. J. Percival, D. M. Wilmouth, P. H. Wine, Chemical Kinetics and Photochemical Data for Use in Atmospheric Studies, Evaluation No. 19 (JPL Publication, 2019); http://jpldataeval.jpl.nasa.gov.

55. S. Tilmes, J.-F. Lamarque, L. K. Emmons, D. E. Kinnison, D. Marsh, R. R. Garcia, A. K. Smith, R. R. Neely, A. Conley, F. Vitt, M. Val Martin, H. Tanimoto, I. Simpson, D. R. Blake, N. Blake, Representation of the Community Earth System Model (CESM1) CAM4-chem within the Chemistry-Climate Model Initiative (CCMI). *Geosci. Model Dev.* **9**, 1853–1890 (2016).

56. R. B. Neale, J. Richter, S. Park, P. H. Lauritzen, S. J. Vavrus, P. J. Rasch, M. Zhang, The mean climate of the Community Atmosphere Model (CAM4) in forced SST and fully coupled experiments. *J. Clim.* **26**, 5150–5168 (2013).

57. R. P. Fernandez, A. Carmona-Balea, C. A. Cuevas, J. A. Barrera, D. E. Kinnison, J.-F. Lamarque, C. Blaszczak-Boxe, K. Kim, W. Choi, T. Hay, A.-M. Blechschmidt, A.

Schönhardt, J. P. Burrows, A. Saiz-Lopez, Modeling the sources and chemistry of polar tropospheric halogens (Cl, Br, and I) using the CAM-Chem global chemistry-climate model. *J. Adv. Model. Earth Syst.* **11**, 2259–2289 (2019).

58. T. Berndt, E. H. Hoffmann, A. Tilgner, F. Stratmann, H. Herrmann, Direct sulfuric acid formation from the gas-phase oxidation of reduced-sulfur compounds. *Nat. Commun.* **14**, 4849 (2023).

59. R. Atkinson, D. L. Baulch, R. A. Cox, J. N. Crowley, R. F. Hampson, R. G. Hynes, M. E. Jenkin, M. J. Rossi, J. Troe, Evaluated kinetic and photochemical data for atmospheric chemistry: Volume I - gas phase reactions of O_x, HO_x, NO_x and SO_x species. *Atmos. Chem. Phys.* **4**, 1461–1738 (2004).

60. M. T. Johnson, A numerical scheme to calculate temperature and salinity dependent air-water transfer velocities for any gas. *Ocean Sci.* **6**, 913–932 (2010).

61. F. Gharagheizi, Determination of diffusion coefficient of organic compounds in water using a simple molecular-based method. *Ind. Eng. Chem. Res.* **51**, 2797–2803 (2012).

62. M. Yang, B. W. Blomquist, C. W. Fairall, S. D. Archer, B. J. Huebert, Air-sea exchange of dimethylsulfide in the Southern Ocean: Measurements from SO GasEx compared to temperate and tropical regions. *J. Geophys. Res. Oceans* **116**, 2010JC006526 (2011).

63. M. Yang, P. D. Nightingale, R. Beale, P. S. Liss, B. Blomquist, C. Fairall, Atmospheric deposition of methanol over the Atlantic Ocean. *Proc. Natl. Acad. Sci. U.S.A.* **110**, 20034–20039 (2013).

64. C.-L. Lee, P. Brimblecombe, Anthropogenic contributions to global carbonyl sulfide, carbon disulfide and organosulfides fluxes. *Earth Sci. Rev.* **160**, 1–18 (2016).

65. J. W. Hurrell, J. J. Hack, D. Shea, J. M. Caron, J. Rosinski, A new sea surface temperature and sea ice boundary dataset for the Community Atmosphere Model. *J. Clim.* **21**, 5145–5153 (2008).

66. W.-L. Wang, G. Song, F. Primeau, E. S. Saltzman, T. G. Bell, J. K. Moore, Global ocean dimethyl sulfide climatology estimated from observations and an artificial neural network. *Biogeosciences* **17**, 5335–5354 (2020).

67. D. Joge, A. S. Mahajan, S. Hulswar, C. A. Marandino, M. Galí, T. G. Bell, M. Yang, R. Simó, Dimethyl sulfide (DMS) climatologies, fluxes, and trends—Part 2: Sea-air fluxes. *Biogeosciences* **21**, 4453–4467 (2024).

68. A. Lana, T. G. Bell, R. Simó, S. M. Vallina, J. Ballabrera-Poy, A. J. Kettle, J. Dachs, L. Bopp, E. S. Saltzman, J. Stefels, J. E. Johnson, P. S. Liss, An updated climatology of surface dimethlysulfide concentrations and emission fluxes in the global ocean. *Global Biogeochem. Cycles* **25**, 2010GB003850 (2011).

69. J.-E. Tesdal, J. R. Christian, A. H. Monahan, K. von Salzen, Evaluation of diverse approaches for estimating sea-surface DMS concentration and air–sea exchange at global scale. *Environ. Chem.* **13**, 390–412 (2015).

70. T. G. Bell, S. Landwehr, S. D. Miller, W. J. de Bruyn, A. H. Callaghan, B. Scanlon, B. Ward, M. Yang, E. S. Saltzman, Estimation of bubble-mediated air-sea gas exchange from concurrent DMS and CO_2 transfer velocities at intermediate-high wind speeds. *Atmos. Chem. Phys.* **17**, 9019–9033 (2017).

71. S. J. Ghan, Technical Note: Estimating aerosol effects on cloud radiative forcing. *Atmos. Chem. Phys.* **13**, 9971–9974 (2013).

72. A. A. Lacis, J. E. Hansen, G. L. Russell, V. Oinas, J. Jonas, The role of long-lived greenhouse gases as principal LW control knob that governs the global surface temperature for past and future climate change. *Tellus B Chem. Phys. Meteorol.* **65**, 19734 (2013).

73. M. J. Iacono, J. S. Delamere, E. J. Mlawer, M. W. Shephard, S. A. Clough, W. D. Collins, Radiative forcing by long-lived greenhouse gases: Calculations with the AER radiative transfer models. *J. Geophys. Res. Atmos.* **113**, 2008JD009944 (2008).